ELSEVIER

Contents lists available at ScienceDirect

### Analytica Chimica Acta

journal homepage: www.elsevier.com/locate/aca



## Near-electrode pH change for voltammetric detection of insoluble lead carbonate



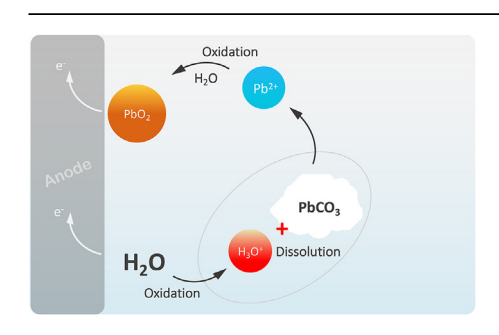
Artur Huseinov, Benjamin L. Weese, Brody J. Brewer, Noe T. Alvarez \*

Department of Chemistry, University of Cincinnati, Cincinnati, OH, 45221, United States

#### HIGHLIGHTS

- Near-electrode pH decrease allows for reagentless dissolution of lead carbonate.
- Additions of insoluble lead carbonate to the solution increase the voltammetric response, similarly to soluble lead nitrate.
- Voltammetric quantification of insoluble lead carbonate was achieved without sample preparation.

#### G R A P H I C A L A B S T R A C T



#### ARTICLE INFO

Article history:
Received 15 June 2021
Received in revised form
14 September 2021
Accepted 18 September 2021
Available online 20 September 2021

Keywords:
Reagentless method
Cathodic stripping voltammetry
Electrochemical acidification
Lead detection
Lead particulates
Local pH change

#### ABSTRACT

Lead contamination of drinking water is a concern to all inhabitants of old cities where lead pipes and soldering are still present. Simple on-site electrochemical detection methods are promising technologies that have gained attention recently. However, conventional electrochemical techniques only quantify soluble forms of lead in water without accounting for insoluble particulates. Herein, a simple voltammetric technique for quantification of insoluble lead species is reported. Lead carbonate (PbCO<sub>3</sub>) was used as a model compound to show the possibility of detecting particulate lead species directly in solution without chemical treatment. Specifically, electrochemical generation of protons was used as an alternative method to dissolve PbCO<sub>3</sub> and thus obtain a more realistic assessment of lead contamination. Lead was detected using cathodic stripping square wave voltammetry (CSSWV). After applying a high oxidizing potential to the electrode immersed in a PbCO<sub>3</sub> solution with solid PbCO<sub>3</sub> particulates, a significant increase in current was observed as compared to that of a saturated PbCO<sub>3</sub> solution. The signal was proportional to the amount of added PbCO<sub>3</sub>, even when the solubility limit was exceeded. Thus, the combination of a local pH change with CSSWV provides a simple, rapid, and reagentless method for an in-situ detection of insoluble lead species.

© 2021 Elsevier B.V. All rights reserved.

#### 1. Introduction

Lead is well known for its toxicity. In addition to the deleterious effects common to most heavy metals, it was recently shown that

\* Corresponding author. E-mail address: alvarene@ucmail.uc.edu (N.T. Alvarez). lead might also cause Alzheimer's disease [1]. Cardiovascular diseases, particularly hypertension, can also be provoked by this metal [2]. Potential sources of lead poisoning include drinking water. In cities built prior to 1987, pipes, fixtures, and welding materials containing lead were employed regularly in drinking water infrastructure. The Flint water crisis is one of the most notable examples of lead pipes having a significant negative impact on human health

[3,4]. The analytical techniques for lead detection approved by the Environmental Protection Agency (EPA) include inductively coupled plasma mass spectrometry (ICP-MS), inductively coupled plasma atomic emission spectroscopy (ICP-AES), and graphite furnace atomic absorption spectroscopy (GFAAS) [5]. These methods require long sample preparation, the use of corrosive acids, expensive equipment, and trained personnel.

Electrochemical methods are simple, inexpensive, and have high potential for on-site analysis [6,7]. Anodic stripping voltammetry is among the most commonly used electrochemical techniques for the detection of lead, mostly due to its high sensitivity [8–12]. This method is based on the reduction of lead ions (Pb $^{2+}$ ) to form metallic lead on the electrode surface (deposition step) and its consecutive oxidation back to Pb<sup>2+</sup> (stripping step). Several variations of cathodic stripping voltammetry can also be used for lead detection. The first approach, known as adsorptive stripping voltammetry, involves deposition of Pb<sup>2+</sup> on an electrode surface modified with a reagent that forms a complex with lead, followed by reduction of the deposited product to lead metal (stripping step) [13–15]. The second approach involves direct anodic oxidation of Pb<sup>2+</sup> ions to form lead (IV) oxide (PbO<sub>2</sub>) and the consecutive reduction of the product to Pb<sup>2+</sup> ions [16,17]. This method avoids the need to modify the electrode surface. Furthermore, the PbO<sub>2</sub> reduction peak appears at a very high potential [17,18], which may eliminate interference from other electroactive components. A similar analysis can be performed using stripping coulometry [19]. However, these techniques can only detect ions or dissolved complexes and do not account for insoluble particles. In most cases, to obtain accurate and representative results, sample preparation is required to transform all lead species into ionic forms.

In addition to Pb<sup>2+</sup> ions, lead may exist in various nonionic forms (hydroxo complexes, insoluble salts, oxides, complexes with organic ligands, etc.) depending on the matrix composition. For example, in tap water collected from houses with lead pipes or exposed to lead soldering and plumbing fixtures, species such as PbCO<sub>3</sub>, (PbCO<sub>3</sub>)<sub>2</sub>Pb(OH)<sub>2</sub>, PbO, PbO<sub>2</sub>, and Pb<sub>3</sub>O<sub>4</sub> are present [20]. Various ortho- and polyphosphate lead species can also be formed in drinking water [21,22]. Tap water may also contain significant amounts of humic acid [23], which is a strong complexing agent that can easily form soluble complexes with lead and other metal ions [24]. In soil, lead can form insoluble carbonates, sulfates, and

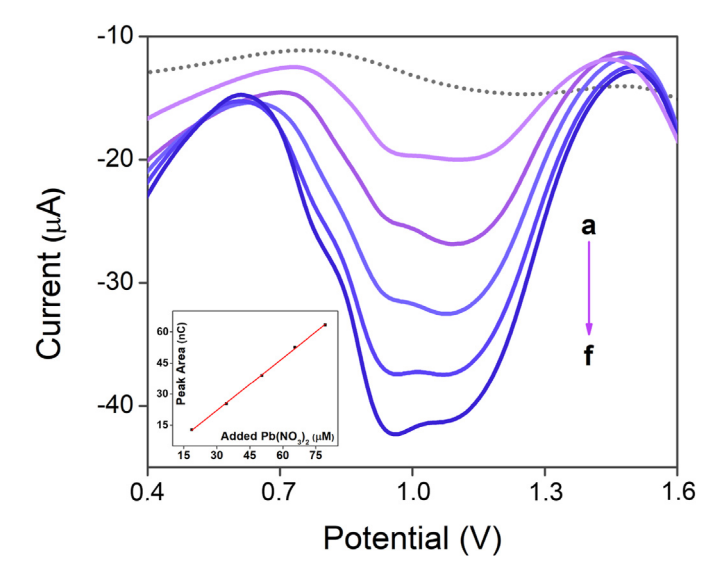


**Fig. 1.** CSVs for different concentrations of Pb(NO<sub>3</sub>)<sub>2</sub> in STW (in  $\mu$ M): (a) 0, (b) 18.6, (c) 34.4, (d) 50.4, (e) 65.4, and (f) 79.3. Inset: calibration graph for Pb(NO<sub>3</sub>)<sub>2</sub> in STW.

chlorides or bind to fulvic, humic, and amino acids [25]. The distribution of these species, in turn, depends on pH [26], and even time of year [27]. Lead carbonate (PbCO<sub>3</sub> or cerussite) is one of the predominant species in water distribution systems [21]. This compound has a very low solubility in water ( $K_s = 7.40 \times 10^{-14}$ ). However, most carbonates, including PbCO<sub>3</sub>, are very soluble in acids. Thus, when the pH decreases, the solubility of PbCO<sub>3</sub> increases significantly.

Electrochemical pH changes can be used to easily control acidity of a solution without the use of additional aggressive reagents. In the case of natural or drinking water, pH changes mostly result from the neutralization of hydrolyzed salts [28]. Separating the cathode and anode with a non-proton exchange membrane allows for the generation of protons (the actual species formed is hydronium ions, H<sub>3</sub>O<sup>+</sup>) at the cathode while simultaneously preventing their oxidation at the anode, which aids in achieving a significant pH drop. This approach has been used in sensors to replace classic solution acidification [29]. A similar technique has also been used for weak acid synthesis [30]. Lacombe et al. reported a reagentless sensor for silicate determination that employs hydrogen ion generation to acidify the solution [31].

In an aqueous solution that contains only an indifferent electrolyte, the protons generated at the cathode move towards the anode, where they will be oxidized, with simultaneous movement of the hydroxyl ions generated at the anode towards the cathode, where they will be reduced. In addition, during migration to the corresponding electrodes, these two species can combine to form water molecules. Therefore, during the electrolysis of such solutions, the bulk pH does not change. However, if proton/hydroxyl ion generation occurs much faster than migration, the pH in the vicinity of the electrode surface can shift, especially in an unstirred solution. This near-electrode change in pH has been studied and even visualized by some authors [32–35].

This work demonstrates the potential of combining a local pH change with CSSWV to quantify lead species that were previously impossible to detect using electroanalytical techniques. Due to its very low solubility, PbCO<sub>3</sub> was chosen as a model compound to show the possibility of detecting insoluble lead species in situ. In this approach, a high oxidizing potential is applied to a platinum electrode to induce the simultaneous oxidation of water and Pb<sup>2+</sup>, producing hydronium ions and PbO<sub>2</sub>, respectively. The hydronium ions chemically react with PbCO<sub>3</sub> in solution to form Pb<sup>2+</sup> ions which undergo oxidation at the anode and are deposited as PbO<sub>2</sub>. Subsequently, cathodic stripping is performed to realize a quantitative voltammetric analysis of deposited PbO<sub>2</sub>. This method is simple, rapid, and requires no sample preparation.

#### 2. Materials and methods

All reagents were purchased from Sigma-Aldrich. The Ag/AgCl reference electrode was obtained from eDAQ Incorporated, and the platinum working electrode (1.651–1626 mm diameter, 99.95% purity) was obtained from Bioanalytical Systems, Inc. All electrochemical measurements were performed using a PalmSens 3 potentiostat (Bioanalytical Systems, Inc).

**Table 1** Areas of PbO $_2$  stripping peaks collected using 43.7  $\mu$ M Pb(NO $_3$ ) $_2$  at different deposition potentials.

Deposition potential, V	Peak area, nC
+2.0	24.8 ± 1.0
+1.8	$23.8 \pm 0.7$
+1.675	$22.0 \pm 0.4$
+1.6	$22.4 \pm 0.1$

# 

Scheme 1. Schematic of the proposed mechanism for PbCO<sub>3</sub> detection. (1) proton generation, (2) PbCO<sub>3</sub> dissolution, (3) PbO<sub>2</sub> deposition, and (4) PbO<sub>2</sub> stripping.

Simulated tap water (STW) was prepared by adjusting the conductivity of Milli-Q water with KNO $_3$  to 420  $\mu$ S cm $^{-1}$ , which approximates the conductivity of tap water in the Cincinnati area, OH, USA. The resulting pH was 6.5. This solution was used as a blank throughout the experiments, unless otherwise stated.

A working solution of Pb(NO<sub>3</sub>)<sub>2</sub> (10.00 mg L<sup>-1</sup>) was prepared by diluting a  $1000 \pm 2$  mg L<sup>-1</sup> Pb(NO<sub>3</sub>)<sub>2</sub> ICP-MS standard with Milli-Q water. An aqueous suspension of PbCO<sub>3</sub> (1.000 g L<sup>-1</sup>) was used to prepare PbCO<sub>3</sub> calibration solutions. Each spike was added immediately after sonication. The reported concentrations of PbCO<sub>3</sub> are referred to the number of moles of PbCO<sub>3</sub> (both solid and dissolved) present in 1 L of the mixture. Saturated solutions of PbCO<sub>3</sub> were obtained by centrifugation (45 min at 4000 rpm; F15–8 × 50cy, Thermo Scientific) of solid PbCO<sub>3</sub> suspended in STW or 0.1 M KNO<sub>3</sub>.

Before use, the platinum working electrode was polished with alumina slurry (d = 0.05  $\mu m$ ). To remove any residual deposits from the electrode, electrochemical cleaning was performed after each measurement by cycling the electrode between -0.3 and + 1.0 V (10 cycles at 0.5 V s $^{-1}$ ) directly in the tested solution. The counter electrode, electrochemical cell, and stirring bar were soaked in nitric acid to remove all possible contaminants.

Cathodic stripping voltammograms (CSVs) were recorded in the range from +1.8 to -0.35 V using the following parameters: deposition potential +1.675 V; deposition time 20 s; quiet time 20 s; potential step 5 mV; amplitude 50 mV; frequency 60 Hz. All potentials were measured vs. Ag/AgCl. The solution was stirred during the deposition step using Fisher Scientific stirring plate at 100 rpm.

The voltammograms were processed using *PSTrace 5.8* software. The values for peak areas were obtained by integrating the i-V traces between two specific potentials. For the blank, the integration was performed between 0.76 V and 1.52 V. Same procedure was used for PbO<sub>2</sub> peaks (the potentials varied as the peak gets broader when lead concentration increases).

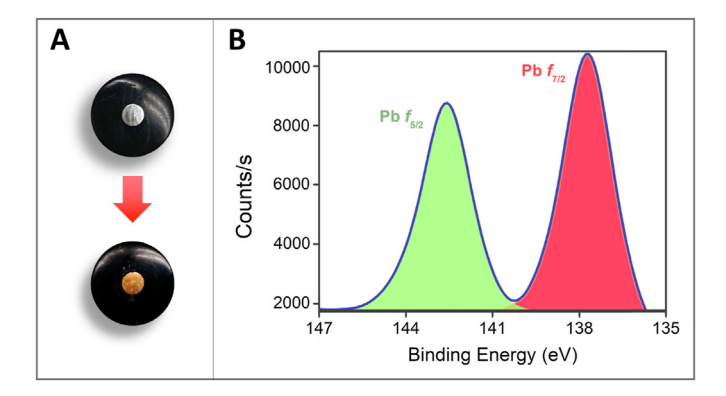


**Fig. 2.** (A) Color change of platinum electrode surface after deposition of PbO $_2$  from an oversaturated PbCO $_3$  solution at +1.675 V for 20 min. (B) XPS spectrum of platinum electrode surface after PbO $_2$  deposition. (For interpretation of the references to colour in this figure legend, the reader is referred to the Web version of this article.)

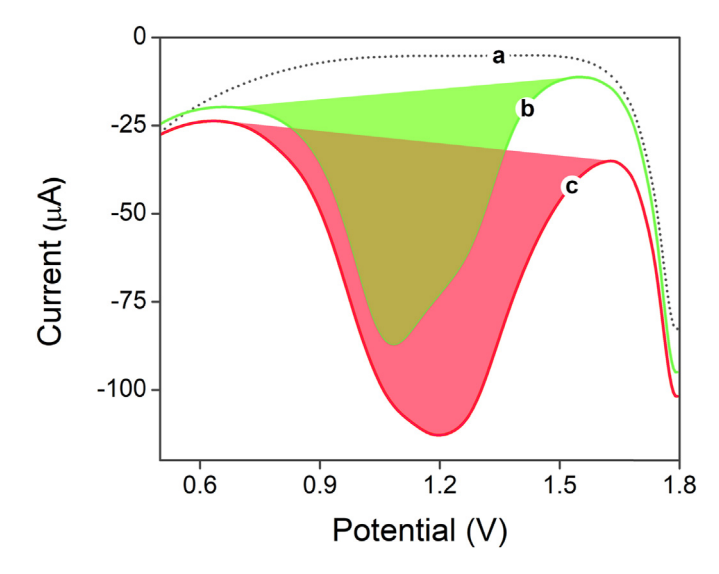


**Fig. 3.** CSVs recorded after 20 min deposition at +1.675 V deposition potential for (a) 0.1 M KNO<sub>3</sub>, (b) saturated PbCO<sub>3</sub> in 0.1 M KNO<sub>3</sub>, and (c) oversaturated PbCO<sub>3</sub> (with solid PbCO<sub>3</sub> particulates) in 0.1 M KNO<sub>3</sub>.

ICP-MS data was collected using an Agilent Technologies 7700 Series ICP-MS system.  $^{209}$ Bi was used as the internal standard. All tested solutions were diluted 1000 times to fit within the calibration range.

X-ray photoelectron spectroscopy (XPS) measurements were

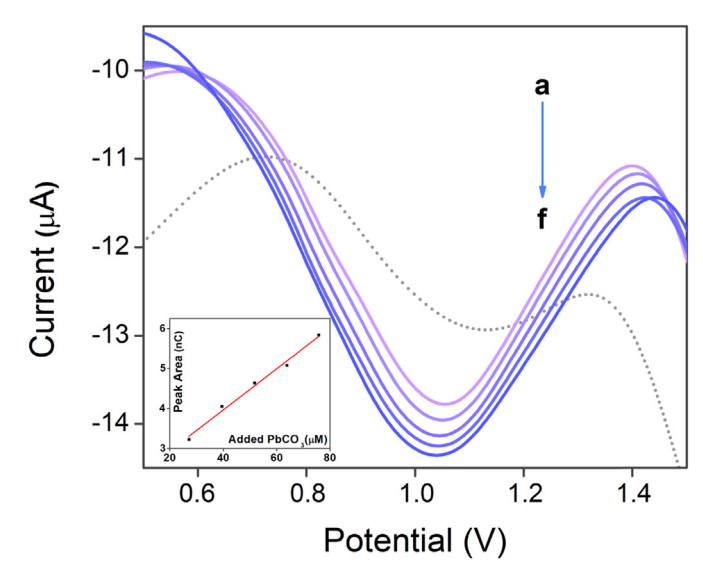


**Fig. 4.** CSVs for different concentrations of PbCO<sub>3</sub> in STW (in  $\mu$ M): (a) 0, (b) 27.2, (c) 39.5, (d) 51.7, (e) 63.8, and (f) 75.8. Inset: calibration graph for PbCO<sub>3</sub> in STW.

performed on a Thermo Fisher Scientific K-alpha system using an Al monochromatic X-ray source (1486.69 eV) and an electron flood gun for charge neutralization. The column pressure was below  $10^{-7}$  Torr. Survey scans were performed at a pass energy of 160 eV, and high-resolution scans were performed at a pass energy of 20 eV. Peak fittings were analyzed using Avantage software.

#### 3. Results and discussion

#### 3.1. Optimization of CSSWV parameters

The stripping peaks of PbO<sub>2</sub> were observed at +1.1 and +0.9 V (Fig. 1). According to Laitinen et al. [19] and Kinard et al. [16], the secondary peak at +0.9 V is due to the stripping of a PbO<sub>2</sub> monolayer from the platinum surface, whereas the peak near +1.1 V represents the stripping of PbO<sub>2</sub> multilayers, one from another. The areas of both peaks increased when more Pb(NO<sub>3</sub>)<sub>2</sub> was added to the solution. The effects of amplitude, frequency, and deposition potential on the PbO2 stripping peaks were studied. First, the amplitude of the square wave was optimized. At amplitudes below 0.005 V, the current ranges were very low, and some distortion of the peak shapes was observed at 0.001 V (Figs. S1A and S1B). At higher amplitudes (0.01 and 0.05 V), the peaks were more intense and well-pronounced (Figs. S1C and S1D). Although increasing the amplitude further resulted in higher currents, the peaks become less pronounced (Figs. S1E and S1F). Thus, 0.05 V was chosen as the optimum amplitude. Varying the frequency had almost no effect on the peak shapes, although it significantly affected the current range (Fig. S2). The frequency associated with the most intense peak (60 Hz) was used for all further measurements. The deposition potential must be sufficient for both Pb<sup>2+</sup> and water oxidation. However, if the potential is too high, oxygen bubbles can form on the electrode and block its electroactive surface. It can be seen from the cyclic voltammogram of STW on a platinum electrode that a sufficient water oxidation current is achieved at potentials higher than +1.4 V (Fig. S3). Fig. S4 shows the CSVs of 43.7  $\mu$ M Pb(NO<sub>3</sub>)<sub>2</sub> recorded at different deposition potentials. In the range from +1.6to +2.0 V, only slight differences in peak areas were observed (Table 1). For all further experiments, a deposition potential of +1.675 V was used (as suggested for PbO2 deposition on a platinum electrode by Zerihun et al. [17]).

#### 3.2. Blank signal

In the CSV of STW, a reduction peak was observed at

approximately +1.1 V (dashed curve, Fig. 1). This signal appeared even without the deposition step, and the peak area remained nearly constant ( $\pm 8\%$ ) after multiple consecutive scans. It is also observed on the CV of STW (inset of Fig. S3). We assumed that this signal results from the reduction of surface platinum oxide species. A possible redox reaction that involves platinum oxide species and occurs around 1.15-1.40 V was described earlier by Jerkiewicz et al. [36]. A similar faint peak has also been described for PdO<sub>2</sub> reduction [37–39]. For all quantitative measurements, the area of the blank signal was mathematically subtracted from the peak area of any measured signal.

#### 3.3. Quantification of lead ions

For the detection of soluble Pb<sup>2+</sup> ions, a Pb(NO<sub>3</sub>)<sub>2</sub> solution was used. The calibration range was chosen based on the solubility of PbCO<sub>3</sub>, as it was the species of interest. It was necessary to explore whether a quantitative relationship exists between the signal and the lead concentration in the range that exceeds the solubility limit of PbCO<sub>3</sub>. Using ICP-MS, the solubility of PbCO<sub>3</sub> in STW was determined to be 13.7  $\pm$  1.1  $\mu$ M. Therefore, the calibration graph for Pb(NO<sub>3</sub>)<sub>2</sub> was constructed in the range of 18.6–79.3  $\mu$ M (*Peak Area* = -(0.64  $\pm$  0.22) + (0.169  $\pm$  0.004)  $\times$  C<sub>Pb(NO<sub>3</sub>)<sub>2</sub>; R<sup>2</sup> = 0.9993).</sub>

#### 3.4. Mechanism of PbCO<sub>3</sub> detection

PbCO $_3$  was chosen as a model compound to show the possibility of using CSSWV for the quantitative analysis of insoluble lead species. The deposition potential of +1.675 V is high enough to induce water oxidation (Equation (1)). As a result, hydronium ions form at the anode. We assume that PbCO $_3$  particulates chemically interact with hydronium ions (Equation (2)), yielding Pb $^{2+}$  ions that undergo further oxidation (Equation (3)). During the stripping step, deposited PbO $_2$  is reduced (Equation (4)). A schematic illustration of the proposed mechanism is shown in Scheme 1.

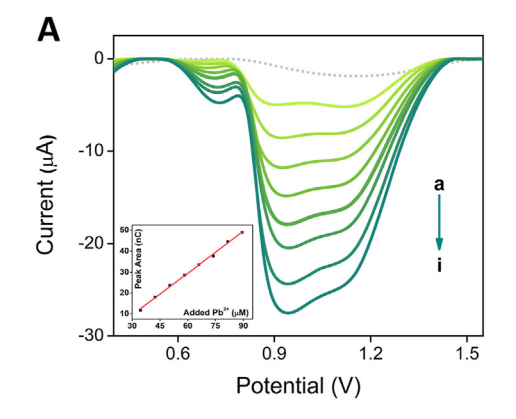
$$6H_2O \to O_2 + 4H_3O^+ + 4e^- \tag{1}$$

$$PbCO_3 + H_3O^+ \rightarrow Pb^{2+} + HCO_3^- + H_2O$$
 (2)

$$Pb^{2+} + 6H_2O \rightarrow PbO_2 + 4H_3O^+ + 4e^-$$
 (3)

$$PbO_2 + 4H_3O^+ + 2e^- \rightarrow Pb^{2+} + 6H_2O$$
 (4)

To show that  $PbO_2$  can be formed from  $PbCO_3$ , the platinum electrode was immersed in 5 mM  $PbCO_3$  in STW, and then a



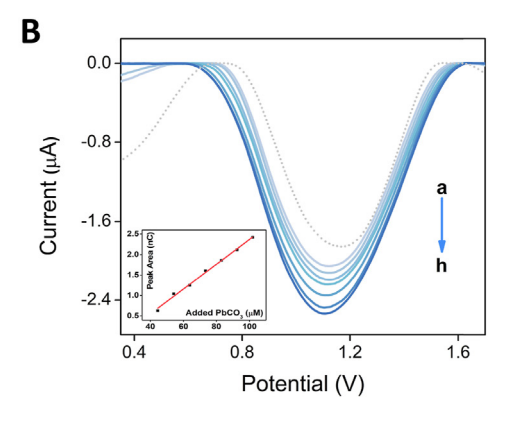


**Fig. 5.** (A) CSVs for different concentrations of Pb(NO<sub>3</sub>)<sub>2</sub> in tap water (in  $\mu$ M): (a) 0, (b) 34.5, (c) 42.4, (d) 50.3, (e) 58.2, and (f) 66.0, (g) 73.8, (h) 81.6, (i) 89.4. Inset: calibration graph for Pb(NO<sub>3</sub>)<sub>2</sub> in tap water; (B) CSVs for different concentrations of PbCO<sub>3</sub> in tap water (in  $\mu$ M): (a) 0, (b) 44.4, (c) 54.1, (d) 63.8, (e) 73.4, (f) 82.9, (g) 92.5, (h) 102. Inset: calibration graph for PbCO<sub>3</sub> in tap water.

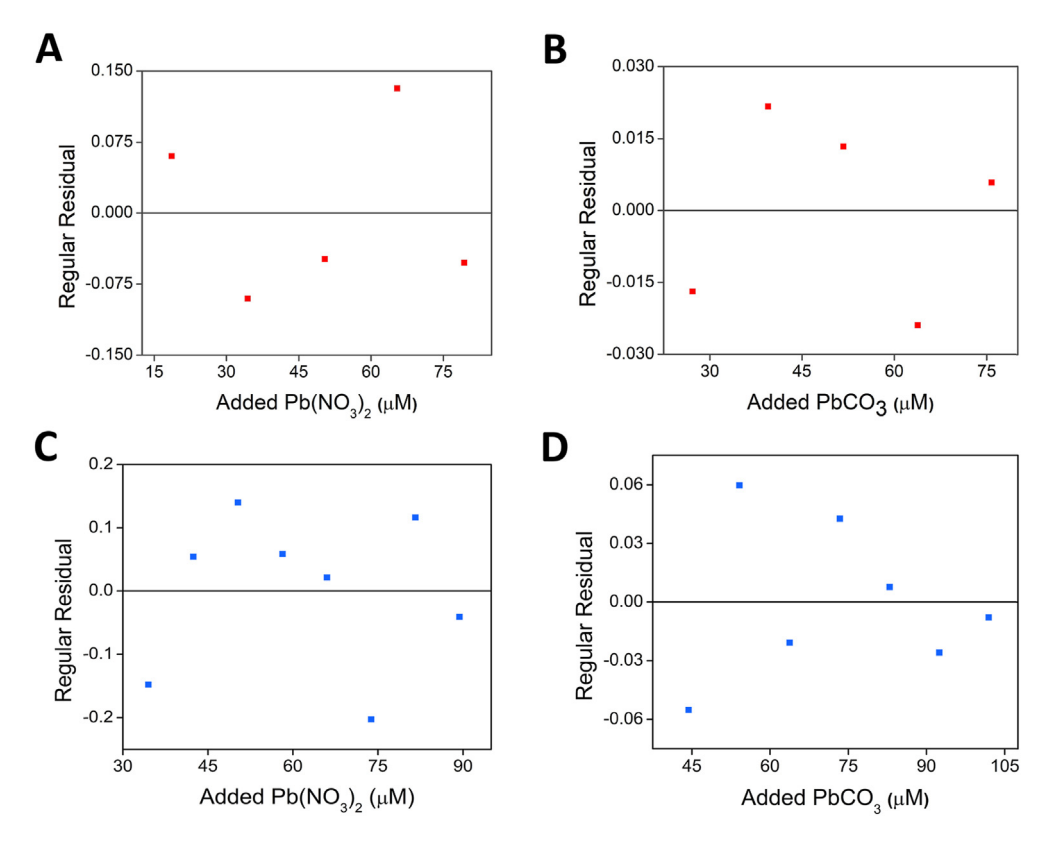


Fig. 6. Regular residual plots for the linear regression of Pb(NO<sub>3</sub>)<sub>2</sub> in STW (A), PbCO<sub>3</sub> in STW(B), Pb(NO<sub>3</sub>)<sub>2</sub> in tap water (C), and PbCO<sub>3</sub> in tap water (D).

**Table 2**Statistical parameters for the calibration graphs.

Calibration graph	V <sub>xo</sub> , %	CQC, %	LOD <sub>3s</sub> , μM	LOQ <sub>10s</sub> , μM
Pb(NO <sub>3</sub> ) <sub>2</sub> in STW	1.3	1.2	0.5	1.8
PbCO <sub>3</sub> in STW	4	2.2	9	29
$Pb(NO_3)_2$ in tap water	4	5	1.0	3
PbCO <sub>3</sub> in tap water	0.4	2.2	23	44

 $V_{xo}$ : standard deviation of the calibration; CQC: calibration quality coefficient;  $LOD_{3s}$ : limit of detection estimated at 3s;  $LOQ_{10s}$ : limit of quantification estimated at 10s.

potential of +1.675 V was applied for 20 min. After deposition, a characteristic brown layer of PbO<sub>2</sub> was formed on the electrode (Fig. 2A and S5). An XPS evaluation of this deposit gave a  $4f_{7/2}$  binding energy of 138.0 eV (referenced to the C1s line), which is very close to the value of 137.9 eV for PbO<sub>2</sub> reported by Morgan et al. [40] (Fig. 2B). The XPS survey spectrum and data are shown in Fig. S6 and Table S1, respectively. A similar deposition experiment was performed using 15.0  $\mu$ M Pb(NO<sub>3</sub>)<sub>2</sub>, which is higher than the concentration of PbCO<sub>3</sub> in a saturated solution. After applying a potential of +1.675 V for 20 min, no deposited product was observed. This finding indicates that in the case of PbCO<sub>3</sub>, solid PbCO<sub>3</sub> dissolves during electrolysis via a chemical reaction, forming significantly more Pb<sup>2+</sup> ions than were initially present in the solution.

To confirm that protons are involved in the transformation of PbCO<sub>3</sub>, CSVs were recorded for saturated and oversaturated (with solid particulates) solutions of PbCO<sub>3</sub> (Fig. 3). As solubility is limited by the solubility constant (at a specific temperature and ionic strength), the initial concentrations of Pb<sup>2+</sup> in both solutions must be equal. Nevertheless, the peak area obtained in the presence of solid PbCO<sub>3</sub> (195  $\pm$  20 nC) was much larger than that for the

saturated solution (127  $\pm$  2 nC), indicating that more PbO<sub>2</sub> was deposited on the electrode. Thus, it was concluded that solid PbCO<sub>3</sub> undergoes dissolution during the deposition step, producing Pb<sup>2+</sup> ions. This occurs as a result of local pH decrease on the surface of platinum electrode, in a similar manner to that reported by Bischoff et al. [33], where major local pH changes were visualized at operando using pH indicators. However, due to the limited proton generation times (20 s) employed in our experiments, no pH changes of the bulk solution were observed. When CSVs were recorded in STW, a significant baseline shift was observed for the oversaturated PbCO<sub>3</sub> solution, thus preventing reliable determination of the peak areas. Consequently, the CSVs in Fig. 3 were obtained using 0.1 M KNO<sub>3</sub> as a blank.

#### 3.5. Quantification of PbCO<sub>3</sub>

Normally, the concentration of lead in drinking water will not exceed the permissible limits of 15  $\mu$ g L<sup>-1</sup> (equivalent to 72 nM of Pb<sup>2+</sup>) required by EPA. PbCO<sub>3</sub> (and other insoluble lead species) in

tap water results from their detachment from lead pipes employed for water transportation. In this case, the concentration of lead ions will significantly increase, as result of PbCO3 dissociation (solubility of PbCO3 under tested conditions was 13.7  $\mu M$ ). Regardless the amount of solid PbCO3, concentration of Pb^2+ produced by PbCO3 dissociation will remain the same. If dissolved lead species were previously present in solution, their concentration would be negligibly small, when compared to the ions resulting from PbCO3 dissociation. Thus, the simultaneous presence of both Pb^2+ and PbCO3 in tap water should not affect the accuracy of the analysis. In case when significant amount of Pb^2+ is already present in water and afterwards a PbCO3 contamination occurs, the accurate quantification will not be possible.

#### 3.6. Quantification of lead ions and PbCO<sub>3</sub> in tap water

The proposed technique was successfully applied for the analysis of a real tap water sample. The tap water sample was used without any previous treatment. The CSV recorded in pure tap water were used as blanks. To construct the calibration graphs for Pb(NO<sub>3</sub>)<sub>2</sub> and PbCO<sub>3</sub>, different amounts of respective species were added in tap water and CSVs were recorded (Fig. 5). For Pb(NO<sub>3</sub>)<sub>2</sub>, the signal was linearly proportional to the Pb(NO<sub>3</sub>)<sub>2</sub> concentration the range of 34.5-89.4 µM (Peak Area  $(2.12 \pm 0.24) + (0.134 \pm 0.004) \times C_{Pb(NO_3)_2}$ ; R<sup>2</sup> = 0.9974). For PbCO<sub>3</sub>, the signal was linearly proportional to the PbCO<sub>3</sub> concentration in of 44.4-102 μΜ (Peak Area  $(0.037 \pm 0.015) + (0.00605 \pm 0.00020) \times C_{PbCO_3}$ ; R<sup>2</sup> = 0.9951). The deviations from linearity below and above the calibration range are shown in Fig. S7B.

#### 3.7. Statistical analysis of the results

All outliers were identified and removed from the data set using the Grubbs test. The signals were measured in triplicate for each calibration solution. Based on these data, repeatability relative standard deviations (RSD<sub>r</sub>) were calculated for Pb(NO<sub>3</sub>)<sub>2</sub> in STW (RSD<sub>r</sub> = 1% at 50.4  $\mu$ M), PbCO<sub>3</sub> in STW (RSD<sub>r</sub> = 6% at 51.7  $\mu$ M), Pb(NO<sub>3</sub>)<sub>2</sub> in tap water (RSD<sub>r</sub> = 0.4% at 58.2  $\mu$ M), and PbCO<sub>3</sub> in tap water (RSD<sub>r</sub> = 4% at 54.1  $\mu$ M). The plots of the regular residuals for all linear regressions have no visible trends but a random spread of data points, thus showing the good linear fits of these curves (Fig. 6).

The quality of each calibration was estimated using the standard deviation of the calibration and the calibration quality coefficient. In each case, these values did not exceed 5%. The limits of detection and limits of quantification were estimated at 3s and 10s, respectively, using the standard deviation of 20 blank signals. All statistical parameters for the calibration graphs are shown in Table 2.

#### 4. Conclusion

Local pH change was successfully applied for near-electrode dissolution of PbCO<sub>3</sub>. Formed lead ions deposited on the electrode surface and contributed to the voltammetric response, thus allowing for the quantification of insoluble PbCO<sub>3</sub>. Three consecutive detections of PbCO<sub>3</sub> in STW and tap water had RSD<sub>r</sub> of 6% (for 51.7  $\mu$ M) and RSD<sub>r</sub> of 4% (at 54.1  $\mu$ M) respectively. The calibration graphs were constructed for cathodic stripping square wave voltammetric detection of PbCO<sub>3</sub> under optimum conditions (amplitude 0.05 V, frequency 60 Hz and deposition potential +1.675 V). The calibration curves possessed good metrological characteristics (both V<sub>x0</sub> and CQC < 5%) in the range of 27.2–75.8  $\mu$ M for STW and 44.4–102  $\mu$ M for tap water. The proposed approach is simple, reagent-free and allows for an in-situ detection of insoluble PbCO<sub>3</sub>.

#### **CRediT authorship contribution statement**

**Artur Huseinov:** Conceptualization, Methodology, Formal analysis, Data curation, Investigation, Writing — original draft, Visualization. **Benjamin L. Weese:** Investigation, Validation. **Brody J. Brewer:** Investigation. **Noe T. Alvarez:** Conceptualization, Resources, Writing — review & editing, Supervision, Project administration, Funding acquisition.

#### **Declaration of competing interest**

The authors declare that they have no known competing financial interests or personal relationships that could have appeared to influence the work ported in this paper.

#### Acknowledgements

The authors would like to thank William Heineman for discussion and feedback, and Julio Landero for his assistance with ICP-MS analysis. Finally, authors thank to NSF 2016484 grant under the NSF PFI-RP program.

#### Appendix A. Supplementary data

Supplementary data to this article can be found online at https://doi.org/10.1016/j.aca.2021.339087.

#### References

- [1] S. Wu, H. Liu, H. Zhao, X. Wang, J. Chen, D. Xia, C. Xiao, J. Cheng, Z. Zhao, Y. He, Environmental lead exposure aggravates the progression of Alzheimer's disease in mice by targeting on blood brain barrier, Toxicol. Lett. 319 (2020) 138–147, https://doi.org/10.1016/j.toxlet.2019.11.009.
- [2] A. Navas-Acien, E. Guallar, E.K. Silbergeld, S.J. Rothenberg, Lead exposure and cardiovascular disease — a systematic review, Environ. Health Perspect. 115 (2007) 472–482, https://doi.org/10.1289/ehp.9785.
- [3] M. Hanna-Attisha, J. LaChance, R.C. Sadler, A. Champney Schnepp, Elevated blood lead levels in children associated with the flint drinking water crisis: a spatial analysis of risk and public health response, Am. J. Publ. Health 106 (2016) 283—290, https://doi.org/10.2105/AIPH.2015.303003.
- [4] K.J. Pieper, M. Tang, M.A. Edwards, Flint water crisis caused by interrupted corrosion control: investigating "ground zero" home, Environ. Sci. Technol. 51 (2017) 2007–2014. https://doi.org/10.1021/acs.est.6b04034.
- [5] K. Deibler, P. Basu, Continuing issues with lead: recent advances in detection, Eur. J. Inorg. Chem. 2013 (2013) 1086–1096, https://doi.org/10.1002/ ejic.201200997.
- [6] O. Akoto, J. Adiyiah, Chemical analysis of drinking water from some communities in the Brong Ahafo region, Int. J. Environ. Sci. Technol. 4 (2007) 211–214, https://doi.org/10.1007/BF03326276.
- [7] P. Gupta, K. Tsai, C.K. Ruhunage, V.K. Gupta, C.E. Rahm, D. Jiang, N.T. Alvarez, True picomolar neurotransmitter sensor based on open-ended carbon nanotubes, Anal. Chem. 92 (2020) 8536–8545, https://doi.org/10.1021/ acs.analchem.0c01363.
- [8] E. Fischer, C.M. van den Berg, Anodic stripping voltammetry of lead and cadmium using a mercury film electrode and thiocyanate, Anal. Chim. Acta 385 (1999) 273–280, https://doi.org/10.1016/S0003-2670(98)00582-0.
- [9] R. Sivasubramanian, M.V. Sangaranarayanan, Detection of lead ions in picomolar concentration range using underpotential deposition on silver nanoparticles-deposited glassy carbon electrodes, Talanta 85 (2011) 2142–2147, https://doi.org/10.1016/j.talanta.2011.07.057.
- [10] D. Zhao, X. Guo, T. Wang, N. Alvarez, V.N. Shanov, W.R. Heineman, Simultaneous detection of heavy metals by anodic stripping voltammetry using carbon nanotube thread, Electroanalysis 26 (2014) 488–496, https://doi.org/10.1002/elan.201300511.
- [11] D. Zhao, D. Siebold, N.T. Alvarez, V.N. Shanov, W.R. Heineman, Carbon nanotube thread electrochemical cell: detection of heavy metals, Anal. Chem. 89 (2017) 9654–9663, https://doi.org/10.1021/acs.analchem.6b04724.
- [12] P. Gupta, C.E. Rahm, D. Jiang, V.K. Gupta, W.R. Heineman, G. Justin, N.T. Alvarez, Parts per trillion detection of heavy metals in as-is tap water using carbon nanotube microelectrodes, Anal. Chim. Acta 1155 (2021) 338353, https://doi.org/10.1016/j.aca.2021.338353.
- [13] C.M.G. Van Den Berg, Determination of copper, cadmium and lead in seawater by cathodic stripping voltammetry of complexes with 8-hydroxyquinoline, J. Electroanal. Chem. Interfacial Electrochem. 215 (1986) 111–121, https://doi.org/10.1016/0022-0728(86)87009-7.
- [14] K. Yokoi, A. Yamaguchi, M. Mizumachi, T. Koide, Direct determination of trace

- concentrations of lead in fresh water samples by adsorptive cathodic stripping voltammetry of a lead-Calcein Blue complex, Anal. Chim. Acta 316 (1995) 363—369, https://doi.org/10.1016/0003-2670(95)00375-A.
- [15] E. Fischer, C.M.G. Van Den Berg, Determination of lead complexation in lake water by cathodic stripping voltammetry and ligand competition, Anal. Chim. Acta 432 (2001) 11–20, https://doi.org/10.1016/S0003-2670(00)01353-2.
- [16] J.T. Kinard, R.C. Propst, Determination of lead at the parts per billion level by cathodic stripping analysis, Anal. Chem. 46 (1974) 1106–1109, https:// doi.org/10.1021/ac60344a020.
- [17] T. Zerihun, P. Gründler, Electrically heated cylindrical microelectrodes. determination of lead on pt by cyclic voltammetry and cathodic stripping analysis, J. Electroanal. Chem. 415 (1996) 85–88, https://doi.org/10.1016/ S0022-0728(96)04711-0.
- [18] T. Ishiyama, K.I. Abe, T. Tanaka, A. Mizuike, Determination of trace lead in copper by cathodic stripping voltammetry, Anal. Sci. 12 (1996) 263–265, https://doi.org/10.2116/analsci.12.263.
- [19] H.A. Laitinen, N.H. Watkins, Cathodic stripping coulometry of lead, Anal. Chem. 47 (1975) 1352–1358, https://doi.org/10.1021/ac60358a055.
- [20] E. Deshommes, L. Laroche, S. Nour, C. Cartier, M. Prévost, Source and occurrence of particulate lead in tap water, Water Res. 44 (2010) 3734–3744, https://doi.org/10.1016/j.watres.2010.04.019.
   [21] J. Zhao, D.E. Giammar, J.D. Pasteris, C. Dai, Y. Bae, Y. Hu, Formation and ag-
- [21] J. Zhao, D.E. Giammar, J.D. Pasteris, C. Dai, Y. Bae, Y. Hu, Formation and aggregation of lead phosphate particles: implications for lead immobilization in water supply systems, Environ. Sci. Technol. 52 (2018) 12612–12623, https://doi.org/10.1021/acs.est.8b02788.
- B.F. Trueman, W.H. Krkošek, G.A. Gagnon, Effects of ortho- and polyphosphates on lead speciation in drinking water, Environ. Sci. Water Res. Technol. 4 (2018) 505–512, https://doi.org/10.1039/C7EW00521K.
   S. Farrah, S. Goyal, C. Gerba, V. Mahajan, C. Wallis, J. Melnick, Concentration of
- [23] S. Farrah, S. Goyal, C. Gerba, V. Mahajan, C. Wallis, J. Melnick, Concentration of humic acid from tapwater, Water Res. 12 (1978) 303–306, https://doi.org/ 10.1016/0043-1354(78)90117-3.
- [24] R. Ernst, H.E. Allen, K.H. Mancy, Characterization of trace metal species and measurement of trace metal stability constants by electrochemical techniques, Water Res. 9 (1975) 969–979, https://doi.org/10.1016/0043-1354(75) 90125-6
- [25] A. Kushwaha, N. Hans, S. Kumar, R. Rani, A critical review on speciation, mobilization and toxicity of lead in soil-microbe-plant system and bioremediation strategies, Ecotoxicol. Environ. Saf. 147 (2018) 1035–1045, https:// doi.org/10.1016/j.ecoenv.2017.09.049.
- [26] G. Sposito, The chemical forms of trace, in: Appl. Environ. Geochemistry, Academic Press, London, 1983, pp. 123–170.
- [27] S. Masters, G.J. Welter, M. Edwards, Seasonal variations in lead release to potable water, Environ. Sci. Technol. 50 (2016) 5269–5277, https://doi.org/ 10.1021/acs.est.5b05060.
- [28] V. Rogov, V. Filipchuk, Electrohimicescoe Izmenenie Svoistv Vodi, Vyshcha

- Shkola, Lviv, 1989.
- [29] J. Jońca, W. Giraud, C. Barus, M. Comtat, N. Striebig, D. Thouron, V. Garçon, Reagentless and silicate interference free electrochemical phosphate determination in seawater, Electrochim. Acta 88 (2013) 165–169, https://doi.org/ 10.1016/j.electacta.2012.10.012.
- [30] I. Sanjuán, V. García-García, E. Expósito, V. Montiel, Paired electrolysis for simultaneous electrochemical water softening and production of weak acid solutions, Electrochem. Commun. 101 (2019) 88–92, https://doi.org/10.1016/ j.elecom.2019.03.002.
- [31] M. Lacombe, V. Garçon, D. Thouron, N. Le Bris, M. Comtat, Silicate electrochemical measurements in seawater: chemical and analytical aspects towards a reagentless sensor, Talanta 77 (2008) 744–750, https://doi.org/10.1016/ j.talanta.2008.07.023.
- [32] N. Fomina, C.A. Johnson, A. Maruniak, S. Bahrampour, C. Lang, R.W. Davis, S. Kavusi, H. Ahmad, An electrochemical platform for localized pH control on demand, Lab Chip 16 (2016) 2236–2244, https://doi.org/10.1039/ C6I.C00421K
- [33] C.F. Bischoff, O.S. Fitz, J. Burns, M. Bauer, H. Gentischer, K.P. Birke, H.-M. Henning, D. Biro, Revealing the local pH value changes of acidic aqueous zinc ion batteries with a manganese dioxide electrode during cycling, J. Electrochem. Soc. 167 (2020), 020545, https://doi.org/10.1149/1945-7111/ab6c57.
- [34] A. Habich, H.R. Hausermann, Demonstration of the pH changes during the electrolysis of water, J. Chem. Educ. 64 (1987) 171, https://doi.org/10.1021/ ed064p171.1.
- [35] A.T. Kuhn, C.Y. Chan, pH changes at near-electrode surfaces, J. Appl. Electrochem. 13 (1983) 189–207, https://doi.org/10.1007/BF00612481.
- [36] G. Jerkiewicz, G. Vatankhah, J. Lessard, M.P. Soriaga, Y.-S. Park, Surface-oxide growth at platinum electrodes in aqueous H2SO4, Electrochim, Acta 49 (2004) 1451–1459, https://doi.org/10.1016/j.electacta.2003.11.008.
- [37] M. Gerstl, M. Joksch, G. Fafilek, The dissolution of palladium as a function of glucose concentration in chloride containing solutions of acidic pH, J. Electroanal. Chem. 741 (2015) 1–7, https://doi.org/10.1016/ i.jelechem.2015.01.009.
- [38] M. Grdeń, M. Łukaszewski, G. Jerkiewicz, A. Czerwiński, Electrochemical behaviour of palladium electrode: oxidation, electrodissolution and ionic adsorption, Electrochim. Acta 53 (2008) 7583-7598, https://doi.org/10.1016/ j.electacta.2008.05.046.
- [39] L.H. Dall'Antonia, G. Tremiliosi-Filho, G. Jerkiewicz, Influence of temperature on the growth of surface oxides on palladium electrodes, J. Electroanal. Chem. 502 (2001) 72–81, https://doi.org/10.1016/S0022-0728(00)00505-2.
- [40] W.E. Morgan, J.R. Van Wazer, Binding energy shifts in the x-ray photoelectron spectra of a series of related Group IVa compounds, J. Phys. Chem. 77 (1973) 964–969, https://doi.org/10.1021/j100626a023.